
Distributed Bayesian clustering

Hanyu Song
Department of Statistical Science
Duke University
Durham, NC 27708
hanyu.song@duke.edu

Yingjian Wang
SAS Institute Inc.
Cary, NC 27513
Yingjian.Wang@sas.com

David Dunson
Department of Statistical Science
Duke University
Durham, NC 27708
dunson@duke.edu

Abstract

In many modern applications, there is interest in analyzing enormous data sets that cannot be easily moved across computers or loaded into memory on a single computer. In such settings, it is very common to be interested in clustering. Existing distributed clustering algorithms are mostly distance or density based without a likelihood specification, precluding the possibility of formal statistical inference. We introduce a nearly embarrassingly parallel algorithm using a Bayesian finite mixture of mixtures model for distributed clustering, which we term distributed Bayesian clustering (DIB-C). DIB-C can flexibly accommodate data sets with various shapes (e.g. skewed or multi-modal). With data randomly partitioned and distributed, we first run Markov chain Monte Carlo in an embarrassingly parallel manner to obtain local clustering draws and then refine across nodes for a final cluster estimate based on *any* loss function on the space of partitions. DIB-C can also provide a posterior predictive distribution, estimate cluster densities, and quickly classify new subjects. Both simulation studies and real data applications show superior performance of DIB-C in terms of robustness and computational efficiency.

1 Introduction

Recent technological advances have greatly accelerated data collection processes, leading to explosively growing data sizes. These data sets are often too big to be stored on a single computer and are costly to move across computers. One common query to these data sets is cluster analysis, which seeks to group observations that are cohesive and separated from other groups. Large scale data sets from astronomy, flow cytometry and many other fields raise questions as to how to discover underlying clusters quickly while allowing for statistical inference.

To cluster large scale data sets, parallel and distributed clustering algorithms have been proposed, mostly based on either distance or density without a likelihood specification. Such algorithms include density based distributed clustering [Januzaj et al., 2004], K-Means with MapReduce (PKMeans) [Zhao et al., 2009] and co-clustering with MapReduce [Papadimitriou and Sun, 2008]. These methods, mostly non-parametric, do not have established statistical properties in general.

Preprint. Work in progress.

In contrast to such methods, Bayesian finite mixture models allow simultaneous clustering, density estimation and uncertainty quantification of cluster-specific parameters. Let $\mathcal{Y} = (\mathbf{y}_1, \dots, \mathbf{y}_N)$, $\mathbf{y}_i \in \mathbb{R}^d$ be a sample of size N . The model assumes that $\mathbf{y}_i (i = 1, \dots, N)$ of dimension d is generated from a finite mixture with K exchangeable mixture components:

$$f(y_i|\Theta, \eta) = \sum_{k=1}^K \eta_k f_k(y_i|\theta_k), \quad \Theta = (\theta_1, \dots, \theta_K), \quad (1)$$

where η_k is the weight associated with component k satisfying $\sum_{k=1}^K \eta_k = 1$ and $f_k(y_i|\theta_k)$ is the component density specified by parameter θ_k . A Bayesian model puts priors on the model parameters (e.g. η_k and θ_k) enabling posterior inference. With each component interpreted as a cluster, this model has been successfully applied to many areas, including agriculture, astronomy, bioinformatics, biology, economics, engineering, genetics, etc.

Finite mixture models often require a predetermined K , but the number of clusters is generally unknown. Even though one can fit multiple models with different K and identify the best one based on model selection criteria (e.g. BIC), such a procedure can be time-consuming given a large data set and less appealing than the natural Bayesian approach, which is to treat the *true* number of clusters K_{true} as an unknown parameter to be estimated jointly with the component-specific parameters. Relevant methods include nonparametric Bayesian mixture models and overfitted finite mixture models. In the former category, commonly used models are Dirichlet process (DP) or Pitman-Yor process (PYP) mixtures; both carry an implicit assumption that as the sample size goes to infinity, the number of clusters inevitably tends to infinity with $K_{true} \sim \alpha \log(N)$ [Korwar and Hollander, 1973] and $K_{true} \sim N^\beta$ (Miller and Harrison [2014] and Orbanz [2014]), respectively, where α and $\beta \in [0, 1)$ are constants. This means the posterior under a DP model fails to concentrate at the true number of components for data from a finite mixture. Overfitted finite mixtures instead apply a finite mixture model with the number of components K intentionally set to be greater than the true number of clusters K_{true} . This approach is more useful for data with a moderate number of clusters that does not increase as the number of observations N increases. Setting the prior on η to be $\text{Dir}(e_0)$, Rousseau and Mengersen [2011] studied the asymptotic behavior of its posterior distribution: if $e_0 < d/2$, where d is the dimension of the cluster-specific parameters θ_k , the posterior expectation of the weights associated with empty clusters asymptotically converges to zero.

A critical component of the finite mixture model specification is the choice of kernel. Although the Gaussian distribution is typically used, most data clusters in real world applications deviate from such a simple symmetric choice. Such misspecification can lead to identification of extraneous clusters to improve model fit, which essentially destroys the interpretation of a mixture component as one cluster. A remedy is to instead model each cluster by a finite Gaussian mixture, a model that can accurately approximate a wide class of distributions. However, such an approach encounters major issues in terms of identifiability of the separate components or clusters, so some care is needed in the specification.

Although Bayesian mixture models are appealing in providing uncertainty quantification in clustering and associated inferences, a key disadvantage is the large computational cost, particularly as the sample size grows. Joint posterior distributions typically have an intractable analytic form, and one typically relies on Markov chain Monte Carlo (MCMC) sampling to generate draws from the posterior. Conventional MCMC algorithms are too slow to be practically useful in massive data applications. Their inherently serial nature also poses challenges in constructing a parallel counterpart. *Embarassingly parallel* (EP) MCMC algorithms have been recently developed to deal with this problem (Scott et al., 2016, Neiswanger et al., 2014, Minsker et al., 2014, Srivastava et al., 2015, Wang et al., 2015, Li et al., 2017). The idea is to break the data into subsets, run MCMC in parallel for each subset and then combine the results.

Inspired by embarrassingly parallel MCMC, we propose a distributed Bayesian clustering framework and we term it DIB-C. The general idea is to produce approximate samples of cluster assignments for big data under a finite mixture of mixtures model and identify an optimal cluster estimate based on a decision-theoretic approach. For scalability, we produce samples of cluster assignments in each partition of the data and combine them

for an approximate sample of global cluster allocations. Because clusters describe inherent relationships among all the data points, the independent clustering performed on each subset must be carefully merged. To minimize data transmission, we employ one of the simplest parallel programming paradigms, *master-slave*, and communicate only summary statistics between the master and slave nodes to refine local cluster assignments across all partitions of the data in order to produce global cluster allocations.

Our main contributions lie in developing a decision theoretic approach to identifying a reliable cluster estimate while minimizing data transmission between the master and slaves nodes, a key consideration in distributed computing. Besides significant computational gain, DIB-C exhibits superior clustering performance in comparison to its non-distributed counterpart due to better mixing in MCMC. In addition, DIB-C can accommodate any loss function on the space of partitions for cluster estimation and enables uncertainty quantification of cluster-specific parameters (such as cluster centers), density estimation and quick classification of a new subject. As a side effect, DIB-C also works for semi-supervised clustering: when the true number of clusters is greater than that represented in the labeled data, DIB-C can automatically determine the number of clusters via the use of an overfitted finite mixture model.

The rest of the paper is organized as follows. In Section 2, we review the model and prior specification of finite mixture of mixtures. In Section 3, we describe the DIB-C framework. Section 4 presents extensive experimental results to illustrate the performance of our framework.

2 Model specification: finite mixture of mixtures

Clusters are groups of data points that are cohesive and connected within a group but are separated from other groups. Assume \mathcal{Y} can be partitioned into R non-overlapping subsets, with subset r , denoted by \mathcal{Y}_r , residing on slave node r ($r = 1, \dots, R$). We follow Malsiner-Walli et al. [2017] (henceforth MWFSG)’s Bayesian finite mixture of Gaussian mixtures (FMGM) for clustering. Assume each component distribution $f_k(\mathbf{y}_i|\theta_k)$ in (1) is a mixture of L Gaussian subcomponents:

$$f_k(\mathbf{y}_i|\theta_k) = \sum_{l=1}^L \omega_{kl} p(y_i | \mu_{kl}, \Sigma_{kl}), \quad (2)$$

where $\theta_k = \{\omega_{kl}, \mu_{kl}, \Sigma_{kl}\}_{l=1}^L$ and $p(y_i | \mu_{kl}, \Sigma_{kl})$ are Gaussian densities used to approximate $f_k(\mathbf{y}_i | \theta_k)$. Such a formulation leads to a hierarchy: the upper level (1) captures a heterogeneous population with K different clusters and each cluster corresponds to a mixture component; the lower level (2) approximates each cluster distribution via a mixture of Gaussian densities $p(y_i|\mu_{kl}, \Sigma_{kl})$. To distinguish the upper and lower level components, we adopt the convention in MWFSG to call $f_k(\mathbf{y}_i|\theta_k)$ *cluster distribution k* and $p(y_i|\mu_{kl}, \Sigma_{kl})$ *subcomponent distribution l* in cluster k .

Combining (1) and (2) provides an alternative expression of the likelihood of \mathbf{y}_i :

$$f(\mathbf{y}_i|\Theta, \eta) = \sum_{k=1}^K \sum_{l=1}^L v_{kl} p(y_i|\mu_{kl}, \Sigma_{kl}), \quad (3)$$

where $v_{kl} = \eta_k \omega_{kl}$. (3) is invariant to permutations of the $K \cdot L$ subcomponents: exchanging subcomponents between clusters does not alter the likelihood, but goes contrary to the general characterization of data clusters, which is a densely connected cloud of data points far away from other densely connected ones. To incorporate such structure, MWFSG proposed a two-level hierarchical prior that repulses the cluster centers and attracts subcomponent means towards the cluster centers. Additionally, since cluster structure is invariant to the ordering of both clusters and subcomponents within a cluster, symmetric priors should be used for clusters on the upper and lower level, respectively, to ensure exchangeability.

Let $\varphi_0 = (e_0, d_0, c_0, g_0, \mathbf{G}_0, \mathbf{B}_0, \mathbf{m}_0, \mathbf{M}_0, \nu)$ be a set of fixed hyper-parameters. The priors at the cluster level are specified so that the K clusters are exchangeable:

$$p(\eta, \theta_1, \dots, \theta_K | \varphi_0) = p(\eta | e_0) \prod_{k=1}^K p(\theta_k | \varphi_0), \quad (4)$$

where $\eta | e_0 \sim \text{Dir}_K(e_0)$, and $\theta_k | \varphi_0$ are independent and identically distributed a priori.

Within each cluster k , the prior distribution can be factored as:

$$p(\theta_k | \varphi_0) = p(w_k | d_0) p(\mu_{k1}, \mu_{k2}, \dots, \mu_{kL} | \mathbf{B}_0, \mathbf{m}_0, \mathbf{M}_0, \nu) p(\Sigma_{k1}, \Sigma_{k2}, \dots, \Sigma_{kL} | c_0, g_0, \mathbf{G}_0), \quad (5)$$

where $\omega_k | d_0 \stackrel{iid}{\sim} \text{Dir}_L(d_0)$, $\mu_{k1}, \dots, \mu_{kL}$ are independently distributed conditional on $\mathbf{B}_0, \mathbf{m}_0, \mathbf{M}_0, \nu$, and $\Sigma_{k1}, \dots, \Sigma_{kL}$ are independent conditional on c_0, g_0, \mathbf{G}_0 .

To create the conditional independence in (4) and (5), MWFSG formulated hierarchical ‘‘random effects’’ priors: first the cluster-specific parameters $(\mathbf{C}_{0k}, \mathbf{b}_{0k}, \Lambda_k)$ are drawn from the same set of distributions and then, conditional on these, the subcomponent-specific parameters $(\mu_{kl}, \Sigma_{kl})_{l=1}^L$ within cluster k are drawn from another set of distributions for all k .

Specifically, cluster-specific parameters $(\mathbf{C}_{0k}, \mathbf{b}_{0k})$ and $\Lambda_k = \text{diag}(\lambda_{k1}, \dots, \lambda_{kd})$, $k = 1, \dots, K$ are drawn from:

$$\begin{aligned} \mathbf{C}_{0k} | g_0, \mathbf{G}_0 &\sim \text{W}_d(g_0, \mathbf{G}_0), \\ \mathbf{b}_{0k} | \mathbf{m}_0, \mathbf{M}_0 &\sim \text{N}_d(\mathbf{m}_0, \mathbf{M}_0), \\ (\lambda_{k1}, \dots, \lambda_{kd}) | \nu &\sim \text{Ga}(\nu, \nu), \end{aligned}$$

where \mathbf{m}_0 is the overall data center. Cluster centers \mathbf{b}_{0k} are generated around \mathbf{m}_0 with \mathbf{M}_0 controlling the shrinkage of \mathbf{b}_{0k} towards \mathbf{m}_0 . MWFSG set $\mathbf{M}_0 \gg \mathbf{S}_y$, where \mathbf{S}_y is the sample covariance of all data so that cluster centers lie relatively far from each other.

Conditional on the cluster-specific random hyperparameters $(\mathbf{C}_{0k}, \mathbf{b}_{0k}, \Lambda_k)$ and the fixed lower level hyperparameters (\mathbf{B}_0, c_0) , the L subcomponent means μ_{kl} and covariance matrices Σ_{kl} are drawn independently for all $l = 1, \dots, L$:

$$\begin{aligned} \mu_{kl} | \mathbf{B}_0, \mathbf{b}_{0k}, \Lambda_k &\sim \text{N}_d(\mathbf{b}_{0k}, \sqrt{\lambda_k} \mathbf{B}_0 \sqrt{\lambda_k}), \\ \Sigma_{kl}^{-1} | c_0, \mathbf{C}_{0k} &\sim \text{W}_d(c_0, \mathbf{C}_{0k}). \end{aligned} \quad (6) \quad (7)$$

μ_{kl} ($l = 1, \dots, L$) should be close to the cluster center \mathbf{b}_{0k} to ensure no gaps among subcomponents and Σ_{kl} ($l = 1, \dots, L$) should be diffuse so that the boundary or outlier points can be well fitted. Therefore, we need \mathbf{B}_0 to impose strong shrinkage of μ_{kl} 's toward \mathbf{b}_{0k} and c_0 to be small to induce large variances in Σ_{kl} 's while permitting large variation of Σ_{kl} 's.

To elicit the prior, MWFSG decomposes the variation of an observation \mathbf{y} into three sources:

$$\begin{aligned} \text{cov}(\mathbf{y}) &= \underbrace{\sum_{k=1}^K \eta_k \Sigma_k}_{\text{within cluster variation}} + \underbrace{\sum_{k=1}^K \eta_k \mu_k \mu_k' - \mu \mu'}_{\text{between cluster variation}} \\ &= \underbrace{\sum_{k=1}^K \eta_k \sum_{l=1}^L \omega_{kl} \Sigma_{kl}}_{\text{within subcomponent variation}} + \underbrace{\sum_{k=1}^K \left(\sum_{l=1}^L \omega_{kl} \mu_{kl} \mu_{kl}' - \mu_k \mu_k' \right)}_{\text{within cluster, between subcomponent variation}} \\ &\quad + \underbrace{\sum_{k=1}^K \eta_k \mu_k \mu_k' - \mu \mu'}_{\text{between cluster variation}} \\ &:= (1 - \phi_W)(1 - \phi_B) \text{cov}(\mathbf{y}) + \phi_W(1 - \phi_B) \text{cov}(\mathbf{y}) + \phi_B \text{cov}(\mathbf{y}), \end{aligned}$$

where ϕ_B is the proportion of variability explained by the cluster centers μ_k around the overall mean $\mu = \sum_{k=1}^K \eta_k \mu_k$, and ϕ_W is the proportion of total variation explained by

subcomponent means μ_{kl} ($l = 1, \dots, L$) around cluster center $\mu_k = \sum_{l=1}^L \omega_{wl} \mu_{kl}$, for all k . By setting $\phi_B = 0.5$ and $\phi_W = 0.1$, we balance the variation of three sources and can elicit prior parameters accordingly.

3 DIB-C framework

The general idea of the DIB-C framework is to produce approximate MCMC samples of cluster assignments under the assumption of a finite mixture of mixtures model in a distributed computing paradigm. Specifically, we sample cluster assignments in each partition of the data and combine them for approximate samples of global cluster allocations.

Because clusters describe inherent relationships among all the data points, the independent clustering performed on each subset must be carefully merged. To minimize data transmission, we communicate only summary statistics between the master and slaves nodes to refine local cluster assignments across all partitions of the data in order to produce reliable global cluster allocations.

Based on the above discussion, we propose a DIB-C framework that consists of five steps: a. partitioning: randomly partitioning the data \mathcal{Y} and distributing them over R nodes (if they are stored in one machine); b. local clustering: running an embarrassingly parallel MCMC to obtain samples of cluster assignments on each partition of the data based on a finite mixture of mixture model; c. local cluster refinement: refining samples of local clusters via summary statistics sent to the master node; d. global cluster estimation: from refined local cluster assignments, identifying a global cluster estimate that minimizes the expected posterior loss defined on the space of partitions; and e. parameter estimation: conditional on the optimal global cluster estimate drawing model parameters from MCMC and performing inference. Local cluster refinement (step c), global cluster estimation (step d) and parameter estimation (step e) incur a small amount of data transmission between the master and slave nodes. In the rest of this section, we introduce the notations used throughout the paper and elaborate on steps b, c, d and e.

3.1 Notations

We represent any quantity associated with subset or node r by adding a subscript r , $r = 1, \dots, R$. Let the sample size of subset \mathcal{Y}_r be n_r , and $\mathcal{Y}_r = \{y_{r1}, y_{r2}, \dots, y_{r,n_r}\}$. Assume subset \mathcal{Y}_r is distributed to and processed on the slave node r , $r = 1, \dots, R$.

As discussed in Section 2, the finite mixture of mixtures model induces both latent cluster and subcomponent allocations of the data. Let a latent cluster allocation be $\mathbf{c} = (C_1, \dots, C_{k_N})$, where C_j contains indices of the data in the j th cluster and k_N is the number of clusters in \mathcal{Y} of sample size N ; similarly let a latent subcomponent allocation be \mathbf{s} . Alternatively, a latent cluster (resp. subcomponent) allocation can be represented by $\mathbf{c} = (c_1, \dots, c_N)$ (resp. $\mathbf{s} = (s_1, \dots, s_N)$), where $c_i = j$ (resp. $s_i = j$) indicates that data point i belongs to cluster j (resp. subcomponent j).

In a distributed computing paradigm, we also express \mathbf{c} (resp. \mathbf{s}) as $\{\mathbf{c}_1, \dots, \mathbf{c}_R\}$ (resp. $\{\mathbf{s}_1, \dots, \mathbf{s}_R\}$), where \mathbf{c}_r (resp. \mathbf{s}_r) represents a latent cluster (resp. subcomponent) allocation for \mathcal{Y}_r . In local cluster refinement (step b), both \mathbf{s} and \mathbf{c} are refined and updated. Let the updated cluster allocation be $\tilde{\mathbf{c}} := \{\tilde{\mathbf{c}}_1, \dots, \tilde{\mathbf{c}}_R\}$, where $\tilde{\mathbf{c}}_r$ represents the updated cluster allocation based on \mathbf{c}_r .

3.2 Local clustering

Let the overall posterior density given \mathcal{Y} and the r th subset posterior density given \mathcal{Y}_r , $r = 1, \dots, R$ be

$$p(\Theta, \eta | \mathcal{Y}) = \frac{\{\prod_{r=1}^R \prod_{i=1}^{n_r} f(y_{ri} | \Theta, \eta)\} p(\Theta, \eta)}{\int \int \{\prod_{r=1}^R \prod_{i=1}^{n_r} f(y_{ri} | \Theta, \eta)\} p(\Theta, \eta) d\Theta d\eta}, \quad (8)$$

$$p_r(\Theta, \eta | \mathcal{Y}_r) = \frac{\{\prod_{i=1}^{n_r} f(y_{ir} | \Theta, \eta)\} p(\Theta, \eta)}{\int \int \{\prod_{i=1}^{n_r} f(y_{ir} | \Theta, \eta)\} p(\Theta, \eta) d\Theta d\eta}. \quad (9)$$

In our algorithm, we run MCMC on R nodes in parallel based on (9), producing draws from each subset posterior $p_r(\Theta, \eta | \mathcal{Y}_r)$, $r = 1, \dots, R$. To produce draws from $p_r(\Theta, \eta | \mathcal{Y}_r)$, $r = 1, \dots, R$ (or $p(\Theta, \eta | \mathcal{Y})$ in a serial algorithm), we can run a block conditional Gibbs sampler with data augmentation. The sampler alternates between imputing cluster allocations and updating parameters specific to each cluster, with the latter step alternating between imputing subcomponent allocations and updating subcomponent-specific parameters. See Appendix for a detailed sampling scheme. One can, however, adopt any other sampling scheme to improve mixing (such as a collapsed Gibbs sampler) as long as samples of cluster and subcomponent allocations are produced.

3.3 Local cluster refinement

The clustering $\mathbf{c} = \{\mathbf{c}_1, \dots, \mathbf{c}_R\}$, generated from naively combining the clusterings from the subsets, in general does not mimic a sample of cluster allocation from $p(\Theta, \eta | \mathcal{Y})$ for two reasons.

First, the cluster labeling can vary across nodes. Figure 1 shows a sample of local cluster allocations from three different nodes when the data set is partitioned and distributed to 4 nodes. We can see that cluster 9 in subset 1 corresponds to cluster 10 in subset 3. Second, the clustering structure could vary across nodes. For example, a single cluster in one subset (e.g. cluster 1 in subset 1 in Figure 1) can correspond to several smaller ones (e.g. cluster 1 and 3 in subset 2) in another subset. Even worse, a cluster in one subset corresponds to a significant number of, but not all, data points from multiple clusters in another subset. Therefore, an algorithm to adjust samples of local cluster assignments, particularly enabling merging and splitting clusters for handling the second issue, is essential.

Ni et al. [2018] proposed an algorithm for cluster merging using Bayesian nonparametric (BNP) methods in a distributed setting. After running an embarrassingly parallel MCMC, they *freeze* the local clusters, meaning that the observations within each cluster will never be split but possibly merged in the subsequent steps, and randomly divide the frozen clusters into R' nodes, where $R' < R$, for further clustering based on the same BNP model. They iteratively perform the above procedures until the number of frozen clusters is sufficiently small to be clustered in a single node. A deficiency of this algorithm is that if clusters are incorrectly merged at some iteration, then there is no hope of recovering the true clustering structure because they can never be split.

Inspired by Ni et al. [2018], we propose a simple and communication efficient algorithm that permits both cluster merging and splitting. In contrast with Ni et al. [2018], we freeze observations at the subcomponent level, rather than at the cluster level. One big advantage is that heavily overlapping subcomponents provide a natural solution to cluster refinement: we can merge or align the frozen local subcomponents across subsets based on their degrees of overlap and map the updated subcomponent assignments to the cluster level, which results in automatic merges or splits of the clusters. Another advantage, since each subcomponent can be described by a Gaussian distribution, is that the natural model to enable such *joint* grouping is simply a finite mixture of Gaussians; if the distributions of any two subcomponents can be well approximated by a single Gaussian kernel, the subcomponents are likely to be grouped together. In Figure 1, for example, subcomponent 1, 7 and 16 from subset 1, 2 and 3, respectively, are likely to be assigned to the same group due to their high overlap; mapping the group label back to the cluster level results in alignment of cluster labels and automatic merging of cluster 2 and 5 in subset 2, which is shown in Figure 2.

Before further illustrating the algorithm, we define some notation. Since each cluster contains L subcomponents, we index the l th subcomponent in cluster k for subset r by $L(k-1) + l$, $r = 1, \dots, R$ and refer to a *non-empty subcomponent* as an *item*, using the word “item” to distinguish these objects from single observations. Let a partition by item in subset r be $\mathbf{s}_r = (S_{r,1}, \dots, S_{r,\mathcal{L}_r})$, where $S_{r,j}$ contains the indices of data points in the j th item and \mathcal{L}_r is the number of items in subset r , $r = 1, \dots, R$; the total number of items across all subsets is $B = \sum_{r=1}^R \mathcal{L}_r$. Label the index set $S_{1,j}$, i.e. the j th item in subset 1, by j and $S_{r,j}$ by $\sum_{i=1}^{r-1} \mathcal{L}_i + j$ for $r = 2, \dots, R$. Thus the order is $S_{1,1}, S_{1,2}, \dots, S_{1,\mathcal{L}_1}, S_{2,1}, \dots, S_{2,\mathcal{L}_2}, \dots, S_{R,\mathcal{L}_R}$. For the b^{th} item, denote the associated data,

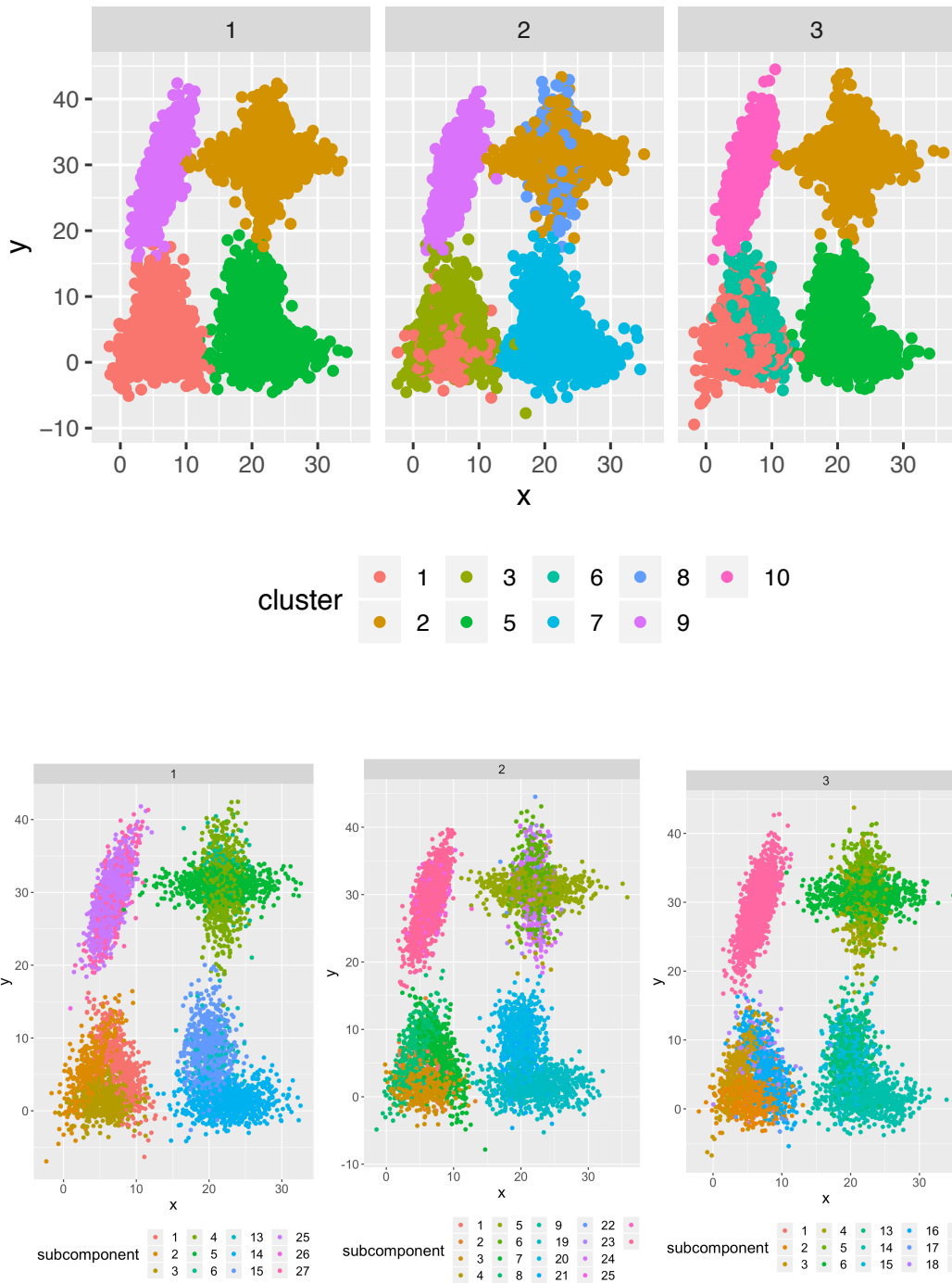


Figure 1: A sample of local clusters (the first row) and subcomponent (the second row) allocation in subset 1, 2 and 3 when the data set is partitioned and run on 4 nodes. 20% randomly selected data points are plotted.

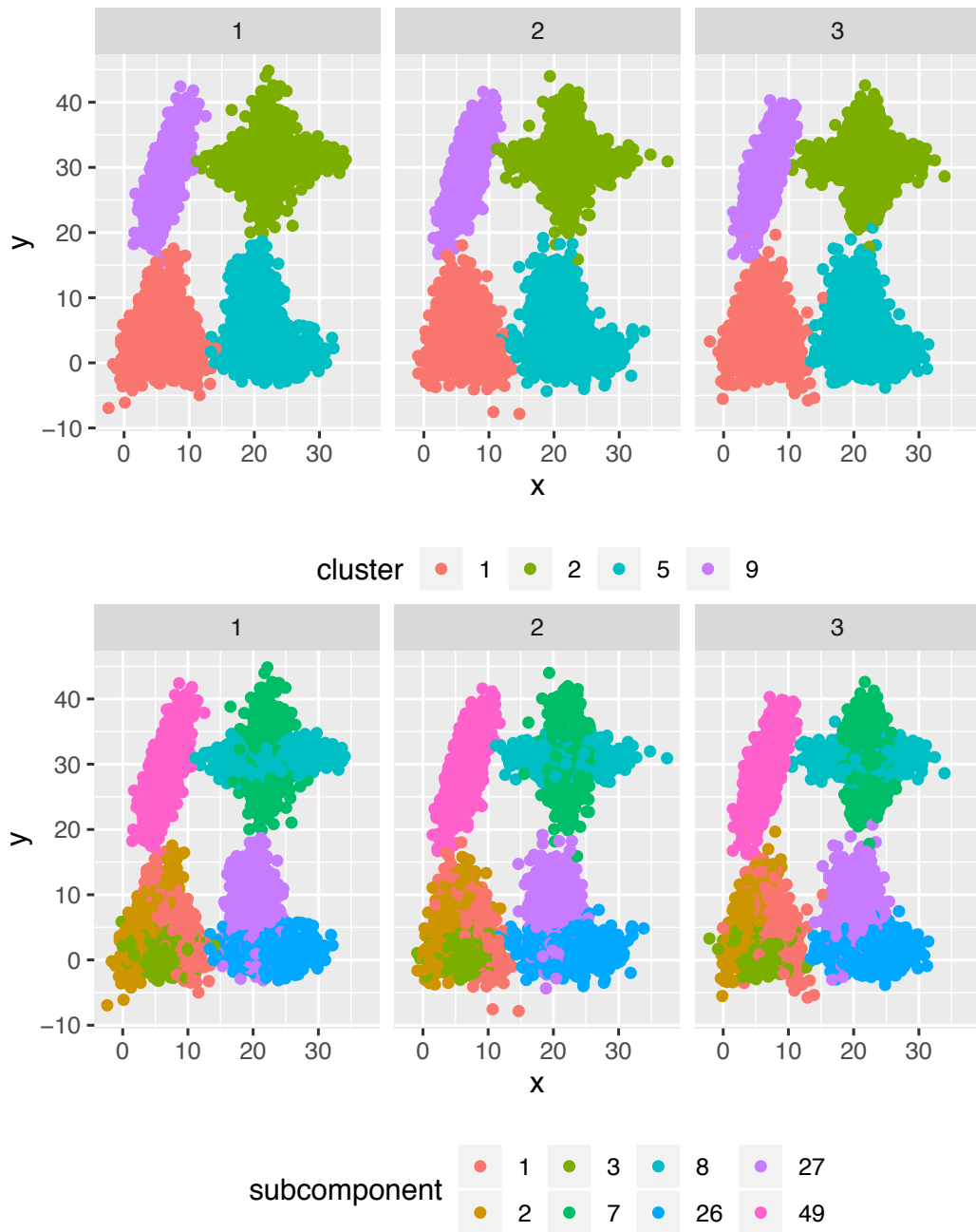


Figure 2: A sample of local clusters (the first row) and subcomponent (the second row) allocation in subset 1, 2 and 3 after applying the refinement algorithm to the outputs shown in Figure 1. 20% randomly selected data points are plotted.

group allocation (to be defined in the next paragraph), sample size, mean and second moment by $\mathbf{y}_b, z_b, n_b, \bar{\mathbf{y}}_b$ and \mathcal{S}_b , respectively, $b = 1, \dots, B$. Let $\mathcal{Y}_h = \{\mathbf{y}_b | z_b = h, b = 1, \dots, B\}$ and its associated sample size, mean and second moment be $N_h, \bar{\mathcal{Y}}_h$ and \mathcal{S}_h , respectively. We use subscript $\setminus b$ to represent the associated quantity with the b th item removed.

To group $\{S_{1,1}, S_{1,2}, \dots, S_{1,\mathcal{L}_1}, S_{2,1}, \dots, S_{2,\mathcal{L}_2}, \dots, S_{R,\mathcal{L}_R}\}$ based on their similarity, we employ a finite mixture of Gaussian model with H components, each of which represents a group:

$$f(\mathbf{y}_b | \Xi, \tau) = \sum_{h=1}^H \tau_h N_h(\mathbf{y}_b | \xi_h), \quad (10)$$

where $\Xi = \{\xi_1, \dots, \xi_H\}$, $\xi_h = \{m_h, \mathcal{C}_h\}$ and $\sum_{h=1}^H \tau_h = 1$.

Placing commonly used conjugate priors on Ξ and τ

$$(\tau_1, \dots, \tau_H) \sim \text{Dir}(\alpha_0, \dots, \alpha_0), \quad (11)$$

$$m_h | \mathcal{C}_h \sim N(\mathbf{0}, \mathcal{C}_h) \quad \text{and} \quad \mathcal{C}_h \sim \text{IW}(\nu_0, \mathbf{S}_0) \quad h = 1, \dots, H, \quad (12)$$

yields a Bayesian model. The refinement procedure is not sensitive to the specific choice of prior parameters because each item contains many observations.

Based on (10), we can derive a *collapsed Gibbs sampler*, where we integrate out the model parameters $\{\Xi, \tau\}$ from the joint posterior and only update the latent group allocation through MCMC sampling; such a sampler in general accelerates convergence to the posterior distribution. The key quantity in updating the group allocation is the posterior probability of item b being assigned to group h :

$$P(z_b = h | \mathbf{z}_{\setminus b}, \mathcal{Y}) \propto P(z_b = h | \mathbf{z}_{\setminus b}) p(\mathbf{y}_b | \mathcal{Y}_{h \setminus b}), \quad h = 1, \dots, H; b = 1, \dots, B. \quad (13)$$

Specifically, the first factor is

$$P(z_b = h | \mathbf{z}_{\setminus b}) = \frac{\Gamma(N + H\alpha_0 - n_b) \Gamma(N_{h \setminus b} + n_b + \alpha_0)}{\Gamma(N + H\alpha_0) \Gamma(N_{h \setminus b} + \alpha_0)}, \quad b = 1, \dots, B, \quad (14)$$

and the second factor is

$$p(\mathbf{y}_b | \mathcal{Y}_{h \setminus b}) = \prod_{j=1}^{n_b} t_d \left(\mathbf{y}_{b,j} \middle| \mathbf{m}_{h \setminus b}, \frac{\kappa_{h \setminus b} + 1}{\kappa_{h \setminus b} (\nu_{h \setminus b} - d + 1) \mathcal{S}_{h \setminus b}}, \nu_{h \setminus b} - d + 1 \right), \quad b = 1, \dots, B, \quad (15)$$

where

$$\begin{aligned} \kappa_{h \setminus b} &= 1 + N_{h \setminus b}, & \nu_{h \setminus b} &= \nu_0 + N_{h \setminus b}, \\ \mathbf{m}_{h \setminus b} &= \frac{N_{h \setminus b} \bar{\mathcal{Y}}_{h \setminus b}}{\kappa_{h \setminus b}} & \text{and} & \quad \mathbf{S}_{h \setminus b} = \mathbf{S}_0 + N_{h \setminus b} \mathcal{S}_{h \setminus b} - \kappa_{h \setminus b} \mathbf{m}_{h \setminus b} \mathbf{m}_{h \setminus b}^T. \end{aligned}$$

The details of the derivation are included in the Appendix. Equation (15) is the joint marginal density of observations in item b , which is a product of t -densities.

Computation of Equations (14) and (15) requires statistics $N_{h \setminus b}, \bar{\mathcal{Y}}_{h \setminus b}, \mathcal{S}_{h \setminus b}, h = 1, \dots, H$, which are just functions of sample size n_b , mean $\bar{\mathbf{y}}_b$ and second moment $\mathcal{S}_b, b = 1, \dots, B$:

$$N_{h \setminus b} = \left(\sum_{i \in b \cup \{j: z_j = h\}} n_i \right) - n_b, \quad (16)$$

$$\bar{\mathcal{Y}}_{h \setminus b} = \left[\left(\sum_{i \in b \cup \{j: z_j = h\}} n_i \bar{\mathbf{y}}_i \right) - n_b \bar{\mathbf{y}}_b \right] / N_{h \setminus b}, \quad (17)$$

$$\mathcal{S}_{h \setminus b} = \left[\left(\sum_{i \in b \cup \{j: z_j = h\}} n_i \mathcal{S}_i \right) - n_b \mathcal{S}_b \right] / N_{h \setminus b}. \quad (18)$$

Therefore, it suffices to have the slaves nodes send these summary statistics, i.e. sample size n_b , mean $\bar{\mathbf{y}}_b$ and second moment \mathcal{S}_b ($b = 1, \dots, B$) to the master node. After $N_{h \setminus b}$, $\bar{\mathcal{Y}}_{h \setminus b}$ and $\mathcal{S}_{h \setminus b}$ ($h = 1, \dots, H$) are evaluated on the master node, they are used to evaluate Equation (14) on the master node, as well as being simultaneously communicated to the slave node $r_b = \{r : \mathbf{y}_b \subset \mathcal{Y}_r, r = 1, \dots, R\}$ to evaluate Equation (15) for $b = 1, \dots, B$, in an embarrassingly parallel manner. The resulting values will again be communicated to the master node for evaluation of Equation (13) for each combination of h and b and an update of latent group allocation z_b , for $b = 1, \dots, B$. Finally, z_b 's are transmitted to the associated slave node $r_b = \{r : \mathbf{y}_b \subset \mathcal{Y}_r, r = 1, \dots, R\}$, where the cluster label of item b is updated to $\lceil \frac{z_b}{L} \rceil$, $b = 1, \dots, B$. Therefore, the updated cluster allocation, denoted by $\tilde{\mathbf{c}}$, is $\{C_{r,j} : j = \lceil \frac{z_b}{L} \rceil, \text{ for } b \text{ that satisfies } \mathbf{y}_b \subset \mathcal{Y}_r\}$, with the combined vector $\tilde{\mathbf{c}} := \{\tilde{\mathbf{c}}_1, \dots, \tilde{\mathbf{c}}_R\}$ considered an approximate sample from $p(\mathbf{c}|\mathcal{Y})$. See Algorithm 1 for clearly outlined steps. We find refining 100 post burn-in iterations of local clustering samples $\mathbf{c} = \{\mathbf{c}_1, \dots, \mathbf{c}_R\}$, as well as running one iteration of refinement starting from \mathbf{c} is sufficient for excellent performance.

Algorithm 1 Algorithm for global cluster alignment

- 1: (Parallel Collapsed Gibbs sampler for an overfitted Gaussian mixture model)
 - 2: **From the worker nodes to the center node:** item size n_b , mean $\bar{\mathbf{y}}_b$ and second moment \mathcal{S}_b , $b = 1, \dots, B$.
 - 3: **On the center node:**
 - 4: Initialize \mathbf{z} by aligning $\bar{\mathbf{y}}_b$ to the closest item from the reference node
 - 5: **for** $h = 1$ to H **do**
 - 6: **for** $b = 1$ to B **do**
 - 7: Evaluate $N_{h \setminus b}$, $\bar{\mathcal{Y}}_{h \setminus b}$, $\mathcal{S}_{h \setminus b}$ and $P(z_b = h|\mathbf{z}_{\setminus b}, \tau)$ using Equation 16, 17, 18 and 14, respectively
 - 8: **Send** $N_{h \setminus b}$, $\bar{\mathcal{Y}}_{h \setminus b}$, $\mathcal{S}_{h \setminus b}$ **and** $P(z_b = h|\mathbf{z}_{\setminus b}, \tau)$ **to the worker node** where item b belongs
 - 9: **end for**
 - 10: **end for**
 - 9: **On the worker nodes:**
 - 10: **parfor** worker node $r = 1$ to R **do**
 - 11: **for** $h = 1$ to H **do**
 - 12: **for** $b = 1$ to \mathcal{L}_r **do**
 - 13: Evaluate $p(\mathbf{y}_b|\mathcal{Y}_{h \setminus b})$ using Equation 15 and **send to the center node**
 - 14: **end for**
 - 15: **end for**
 - 16: **end parfor**
 - 15: **On the center node:**
 - 16: **for** $h = 1$ to H **do**
 - 17: **for** $b = 1$ to B **do**
 - 18: Evaluate $P(z_b = h|\mathbf{z}_{\setminus b}, \mathcal{Y})$ using Equation 13
 - 19: Sample z_b from $P(z_b|\mathbf{z}_{\setminus b}, \mathcal{Y})$ after normalization
 - 20: **Return** z_b **to the worker node** where item b belongs
 - 21: **end for**
 - 22: **end for**
-

Finally, we can use a randomly selected reference node to create consistent labels across the subsets. Specifically, a node $r^* \in \{1, \dots, R\}$ is randomly drawn so that \mathbf{s}_{r^*} serves as the reference to which we jointly align the group allocations z_b ($b = 1, \dots, B$) and then the cluster allocations associated with item b are updated to be $\lceil \frac{z_b}{L} \rceil$, a consistent set of labels used across nodes.

It is possible that items originating from the same cluster are assigned to different groups and end up forming separate clusters. It is also possible that items originating from different clusters are assigned to the same or nearby groups, which become subcomponents of the same cluster. This means that our refinement algorithm is flexible enough to allow both cluster merging and splitting, and is thus less sensitive to the clusters found on the subsets.

3.4 Global cluster estimation

Taking a decision-theoretic approach, we identify the point estimate of clustering \mathbf{c}^* that minimizes the posterior expected loss:

$$\mathbf{c}^* = \arg \min_{\hat{\mathbf{c}}} \mathbb{E}[L(\mathbf{c}, \hat{\mathbf{c}})|\mathcal{Y}]. \quad (19)$$

$\mathbb{E}[L(\mathbf{c}, \hat{\mathbf{c}})|\mathcal{Y}]$ can often be simplified so that it depends on the posterior *only* through the posterior similarity matrix. For example, under Binder's loss $\mathbf{B}(\mathbf{c}, \hat{\mathbf{c}}) = \sum_{n < n'} \mathbb{1}(c_n = c_{n'}) \mathbb{1}(\hat{c}_n \neq \hat{c}_{n'}) + \mathbb{1}(c_n \neq c_{n'}) \mathbb{1}(\hat{c}_n = \hat{c}_{n'})$, $\mathbb{E}[\mathbf{B}(\mathbf{c}, \hat{\mathbf{c}})|\mathcal{Y}] = \sum_{n < n'} (\mathbb{1}(\hat{c}_n = \hat{c}_{n'}) - p(c_n = c_{n'}|\mathcal{Y}))^2$, where $p(c_n = c_{n'}|\mathcal{Y})$ is the posterior probability that data point n and n' belong to one cluster; this quantity can be easily estimated from the posterior similarity matrix. Therefore, a common practice to identify \mathbf{c}^* is through the posterior similarity matrix.

For big data of size N , the N by N posterior similarity matrix would incur both large storage and computational costs, the latter of which is $O(N^2)$ for each iteration in the set \mathcal{T} , where \mathcal{T} contains all the iterations involved in creating the posterior similarity matrix.

Here, we take a different perspective by directly exploiting the loss function definition in estimating the posterior expected loss. The fact that clustering is invariant to the permutation of data point indices implies that a loss function $L(\mathbf{c}, \hat{\mathbf{c}})$ must be a function of the *joint counts* $N_{ij} = |C_i \cap \hat{C}_j|$, which is the number of data points in both C_i , the set of data indices in cluster i under \mathbf{c} and \hat{C}_j , the set of data indices in cluster j under $\hat{\mathbf{c}}$, $i = 1, \dots, k_N$ and $j = 1, \dots, \hat{k}_N$ [Binder, 1978]; these joint counts can be easily obtained through parallel computation. Another advantage of this method is that it can accommodate any loss function defined on the space of partitions, due to its direct use of the definition.

Without loss of generality, we demonstrate our algorithm based on the variation of information (VI) loss. The VI loss is an information theoretic criterion for comparing two clustering structures and is defined as:

$$\begin{aligned} \text{VI}(\mathbf{c}, \hat{\mathbf{c}}) &= H(\mathbf{c}) + H(\hat{\mathbf{c}}) - 2I(\mathbf{c}, \hat{\mathbf{c}}) \\ &= \sum_{i=1}^{k_N} \frac{N_{i+}}{N} \log \left(\frac{N_{i+}}{N} \right) + \sum_{j=1}^{\hat{k}_N} \frac{N_{+j}}{N} \log \left(\frac{N_{+j}}{N} \right) - 2 \sum_{i=1}^{k_N} \sum_{j=1}^{\hat{k}_N} \frac{N_{ij}}{N} \log \left(\frac{N_{ij}}{N} \right), \end{aligned} \quad (20)$$

where H is the entropy function and I is the mutual information [Meilă, 2007]; N_{i+} and N_{+j} represent the counts in C_i under \mathbf{c} and C_j under $\hat{\mathbf{c}}$ respectively. The posterior expected VI loss can be simplified to:

$$\mathbb{E}[\text{VI}(\mathbf{c}, \hat{\mathbf{c}})|\mathcal{Y}] = \sum_{n=1}^N \log \left(\sum_{n'=1}^N \mathbb{1}(\hat{c}_{n'} = \hat{c}_n) \right) - 2 \sum_{n=1}^N \mathbb{E} \left(\log \left(\sum_{n'=1}^N \mathbb{1}(c_{n'} = c_n, \hat{c}_{n'} = \hat{c}_n) \right) | \mathcal{Y} \right) \quad (21)$$

up to a constant. Because estimating Equation (21) is computationally intensive — $O(|\mathcal{T}|N^2)$ for a given clustering candidate $\hat{\mathbf{c}}$, Wade and Ghahramani [2017] upper bounded 21 by $\sum_{n=1}^N \log \left(\sum_{n'=1}^N \mathbb{1}(\hat{c}_{n'} = \hat{c}_n) \right) - 2 \sum_{n=1}^N \log \left(\sum_{n'=1}^N P(c_{n'} = c_n | \mathcal{Y}) \mathbb{1}(\hat{c}_{n'} = \hat{c}_n) \right)$ via Jensen's inequality and had computational cost reduced to $O(N^2)$; this still remains astronomical for our case.

Based on the definition in Equation (20), the posterior expected VI loss can instead be estimated by

$$\mathbb{E}[\widehat{\text{VI}}(\mathbf{c}, \hat{\mathbf{c}})|\mathcal{Y}] = \sum_{j=1}^{\hat{k}_N} \frac{N_{+j}}{N} \log \left(\frac{N_{+j}}{N} \right) - \frac{2}{|\mathcal{T}|} \sum_{t \in \mathcal{T}} \sum_{i=1}^{k_N^{(t)}} \sum_{j=1}^{\hat{k}_N^{(t)}} \frac{N_{ij}^{(t)}}{N} \log \left(\frac{N_{ij}^{(t)}}{N} \right), \quad (22)$$

where \mathcal{T} is the set of iterations under consideration randomly drawn from $\{1, \dots, T\}$. The clustering candidates $\hat{\mathbf{c}}$ are a random subset of $\{1, \dots, T\}$, that is, we randomly draw a set $\mathcal{M} \in \{1, \dots, T\}$ and consider clustering candidates $\hat{\mathbf{c}} \in \{\hat{\mathbf{c}}^{(t)}, t \in \mathcal{M}\}$. The choice of $|\mathcal{T}|$ and

$|\mathcal{M}|$ is at the user's discretion; our experiments show superior clustering performance with $|\mathcal{T}| = 100$ and $|\mathcal{M}| = 20$.

In Equation (22), both $N_{ij}^{(t)}$ and N_{+j} can be computed in parallel, because the refined cluster allocations $\{\tilde{\mathbf{c}}^{(t)}, t = 1, \dots, T\}$ make the following relationships hold:

$$N_{ij}^{(t)} = \sum_{r=1}^R N_{r,ij}^{(t)}, \quad N_{+j} = \sum_{r=1}^R N_{r,+j}. \quad (23)$$

For iteration t , the slave node r first evaluates $N_{r,ij}^{(t)}$ and $N_{r,+j}$ (for $i = 1, \dots, k_N^{(t)}$ and $j = 1, \dots, \hat{k}_N$) in parallel, $r = 1, \dots, R$; such evaluation incurs computational cost $O(nT)$, where $n := \max_r n_r$ the largest sample size on any slave node. The slave nodes then transmit the statistics to the master node; for a clustering candidate with \hat{k}_N clusters, the amount of data communication is $|\mathcal{T}| \hat{k}_N k_N^{(t)} R$, where $k_N^{(t)} \leq K$. Next, the master node evaluates all $N_{ij}^{(t)}$ and N_{+j} based on Equation 23 and then the quantity in Equation 22. The point estimate of the clustering is $\mathbf{c}^* = \arg \min_{\tilde{\mathbf{c}}^{(t)}, t \in \mathcal{M}} \mathbb{E}[\widehat{\text{VI}}(\mathbf{c}, \tilde{\mathbf{c}}^{(t)}) | \mathcal{Y}]$.

3.5 Parameter estimation

Parameter estimation is optional if cluster estimation is the goal, but interests in inference on the cluster-specific quantities or classifying future subjects make it essential. Specifically, to classify a new subject \mathbf{y} , one can use a *Bayes classifier* — evaluating its posterior probability of belonging to cluster j : $P(\mathbf{y} \in \text{cluster } j) = \frac{\eta_j f_j(\mathbf{y} | \theta_j)}{\sum_{k=1}^{k_N} \eta_k f_k(\mathbf{y} | \theta_k)}$, $j = 1, \dots, k_N$ and assigning \mathbf{y} to the cluster that yields the highest posterior probability.

The general idea of our algorithm is to only sample the subcomponent-specific parameters (e.g. ω_{kl} and μ_{kl}) conditional on the aligned subcomponent assignments, allowing the MCMC updates to depend on the data only through summary statistics. These statistics include subcomponent sizes $|i : \tilde{s}_i = l, \tilde{c}_i = k|$, the sum of squares $\sum_{i: \tilde{s}_i = l, \tilde{c}_i = k} y_i y_i^T$ and the data sums $\sum_{i: \tilde{s}_i = l, \tilde{c}_i = k} y_i$, $l = 1, \dots, L$, $k = 1, \dots, k_N$ (see the Appendix for the details of MCMC updates).

Such an approach has several advantages. First, subcomponent assignments are aligned across all subsets through the local cluster refinement algorithm, which makes the following relationships hold:

$$\sum_{i: y_i \in \mathcal{Y}} \mathbb{1}_{\tilde{s}_i = l, \tilde{c}_i = k} = \sum_{r=1}^R \sum_{i: y_i \in \mathcal{Y}_r} \mathbb{1}_{\tilde{s}_i = l, \tilde{c}_i = k}, \quad (24)$$

$$\sum_{\substack{y_i \in \mathcal{Y} \\ \tilde{s}_i = l, \tilde{c}_i = k}} y_i y_i^T = \sum_{r=1}^R \sum_{\substack{y_i \in \mathcal{Y}_r \\ \tilde{s}_i = l, \tilde{c}_i = k}} y_i y_i^T, \quad (25)$$

$$\sum_{\substack{y_i \in \mathcal{Y} \\ \tilde{s}_i = l, \tilde{c}_i = k}} y_i = \sum_{r=1}^R \sum_{\substack{y_i \in \mathcal{Y}_r \\ \tilde{s}_i = l, \tilde{c}_i = k}} y_i, \quad (26)$$

$$l = 1, \dots, L, k = 1, \dots, k_N.$$

Such relationships justify our parallel algorithm: the slave nodes first compute the relevant statistics in parallel and then communicate them to the master node for summing. Such communication only occurs once; because conditional on the subcomponent assignments, the summary statistics are fixed throughout the MCMC updates. Second, the fixed subcomponent assignments and the use of summary statistics significantly reduce computation per iteration and lead to faster convergence due to reduced dependence between iterations. Third, posterior estimates of parameters are often non-identifiable in finite mixture models due to label switching, a phenomenon which occurs when exchangeable priors are placed on the

parameters. It is particularly challenging to resolve, despite many available post-sampling relabeling schemes [Stephens, 2000, Sperrin et al., 2010, Papastamoulis and Iliopoulos, 2010, Papastamoulis, 2014, Rodríguez and Walker, 2014], for overfitted mixture models, as superfluous clusters may merge or overlap with other ones, or be empty. By fixing the latent cluster assignments, we bypass label switching at the cluster level, eliminating the need to post process MCMC outputs.

4 Experiments

In this section, we provide extensive numerical experiments for assessing the performance of DIB-C, as measured by the scalability of the computation time and classification performance with the data size and number of computing nodes. We use training sets of size $N = 12$ thousand, 120 thousand, and 1 million and distribute each data set to clusters ranging in size from 1 to 30 nodes. The test sets contain 3 thousand, 30 thousand, and 250 thousand observations, respectively, i.e. 20% of the total data size. All the experiments were conducted on the Duke Compute Cluster; due to limitations of the cluster, we only benchmark the time of DIB-C up to 30 nodes and performance up to 120 nodes.

When the data are distributed to a single node, local cluster refinement is not necessary; that is, a full MCMC for (local) clustering is immediately followed by (global) cluster estimation. The prior setup is shared by all experiments from the same data set. In the local clustering step, we run 1000 iterations of MCMC across all experiments, with the first 500 being burn-ins. Then we refine 100 iterations of local clustering samples, from which we randomly select 20 to be the clustering candidates considered for the global cluster estimation based on the variation of information loss. To estimate the model parameters, we run 2000 iterations of MCMC conditional on the subcomponent and cluster assignments

4.1 Experimental setup

4.1.1 Synthetic data sets

The simulation setup originated in Baudry et al. [2010] and was later augmented by Malsiner-Walli et al. [2017]. The data sets contain four clusters of varying shapes, including one triangle shape, one L shape, one cross shape and one ellipse. They are generated from an eight-component Gaussian mixture with component means

$$(\mu_1, \dots, \mu_8) = \begin{pmatrix} 6 & 4 & 8 & 22.5 & 20 & 22 & 22 & 6.5 \\ 1.5 & 6 & 6 & 1.5 & 8 & 31 & 31 & 29 \end{pmatrix},$$

covariance matrices

$$\begin{aligned} \Sigma_1 &= \begin{pmatrix} 4.84 & 0 \\ 0 & 2.89 \end{pmatrix}, & \Sigma_2 &= \begin{pmatrix} 3.61 & 5.05 \\ 5.05 & 14.44 \end{pmatrix}, & \Sigma_3 &= \begin{pmatrix} 3.61 & -5.05 \\ -5.05 & 14.44 \end{pmatrix}, & \Sigma_4 &= \begin{pmatrix} 12.25 & 0 \\ 0 & 3.24 \end{pmatrix}, \\ \Sigma_5 &= \begin{pmatrix} 3.24 & 0 \\ 0 & 12.25 \end{pmatrix}, & \Sigma_6 &= \begin{pmatrix} 14.44 & 0 \\ 0 & 2.25 \end{pmatrix}, & \Sigma_7 &= \begin{pmatrix} 2.25 & 0 \\ 0 & 17.64 \end{pmatrix}, & \Sigma_8 &= \begin{pmatrix} 2.25 & 4.20 \\ 4.20 & 16.00 \end{pmatrix}, \end{aligned}$$

cluster weight vectors $\eta = (\frac{1}{4}, \frac{1}{4}, \frac{1}{4}, \frac{1}{4})$ and subcomponent weight vectors $\omega_1 = (\frac{1}{3}, \frac{1}{3}, \frac{1}{3})$, $\omega_2 = (\frac{1}{2}, \frac{1}{2})$, $\omega_3 = (\frac{1}{2}, \frac{1}{2})$, $\omega_4 = 1$. Figure 3 shows a scatter plot of a data set simulated from this setup. In our experiment, we simulate 10 data sets for each sample size. To estimate the model, we let $K = 10$ and $L = 3$.

4.1.2 Flow cytometry data

As a real data application, we consider high-frequency, continuous flow cytometry data collected from particles in aquatic environments by SeaFlow instruments. Specifically, the SeaFlow instruments continuously sample surface seawater, generating a time series of cytometry samples (one every 3 min) containing measurements of the optical properties, including light scatter and intrinsic fluorescence, of small phytoplankton cells during a research cruise [Hyrkas et al., 2015]. The measurements in the data set we use [Armbrust Lab] are forward and perpendicular scatter, and phycoerythrin and chlorophyll levels. One

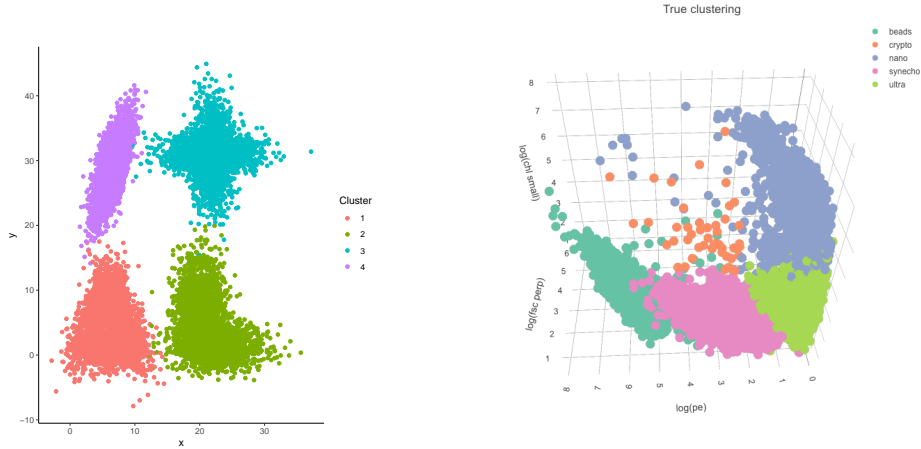


Figure 3: Left: the scatter plot of a synthetic data set simulated with $N = 12,000$ observations; right: the scatter plot of 10,000 observations randomly drawn from the 1 million training set of the flow cytometry data.

important problem of interest is to classify phytoplankton cells based on their optical measurements.

Currently the dominant classification method in this application area is manual gating, i.e. manually identifying the physical boundaries for clusters of cells. This process is subjective and can be infeasible given the massive amount of data collected during a research cruise [Hyrkas et al., 2016]. In addition, properties of the same phytoplankton species may vary as environmental conditions (e.g. daylight) change over time and space [Sosik et al., 2010], leading to varying cluster centers and shapes.

Figure 3 shows a scatter plot of the three variables (i.e. perpendicular scatter, phycoerythrin and chlorophyll) that explain most variation in the data on their logarithmic scales using a random subset from the first one million observations. We notice that synecho, as one species, has visually disjoint components; yet nano and ultra, two distinct species, are not well separated. In addition, crypto is a rare cluster with wide spread. All these factors add to the clustering difficulty.

A recent state-of-the-art clustering method first segments the data based on visual inspection of a change point in cluster formation and independently clusters these segments using a Gaussian mixture model with a pre-determined number of clusters [Hyrkas et al., 2016]. In evaluating the clustering performance, they excluded observations whose assignment probability to any cluster is less than 0.7 and benchmarked the remaining observations against their manually-gated labels; this procedure resulted in an average F-measure of 0.864.

Since handling the time-varying aspect is not our purpose here and given limited computing resources, we only use the first 1.25 million observations from the data set and similarly benchmark against the manually-gated labels. Due to the partially available labels, the training set contains around 3.5% unlabeled data for each data size setting N . These unlabeled data are used in model fitting, but are excluded in clustering performance evaluation.

Our method, in contrast, does not require a pre-determined number of clusters as an input or exclude observations based on their assignment probabilities. Noticing that each variable is *highly* right skewed, we transform the four variables to their logarithmic scales for ease of approximation. We set the upper bound K of the number of clusters to be 8 and the number of subcomponents per cluster L to be 2 for the experiments of the flow cytometry data.

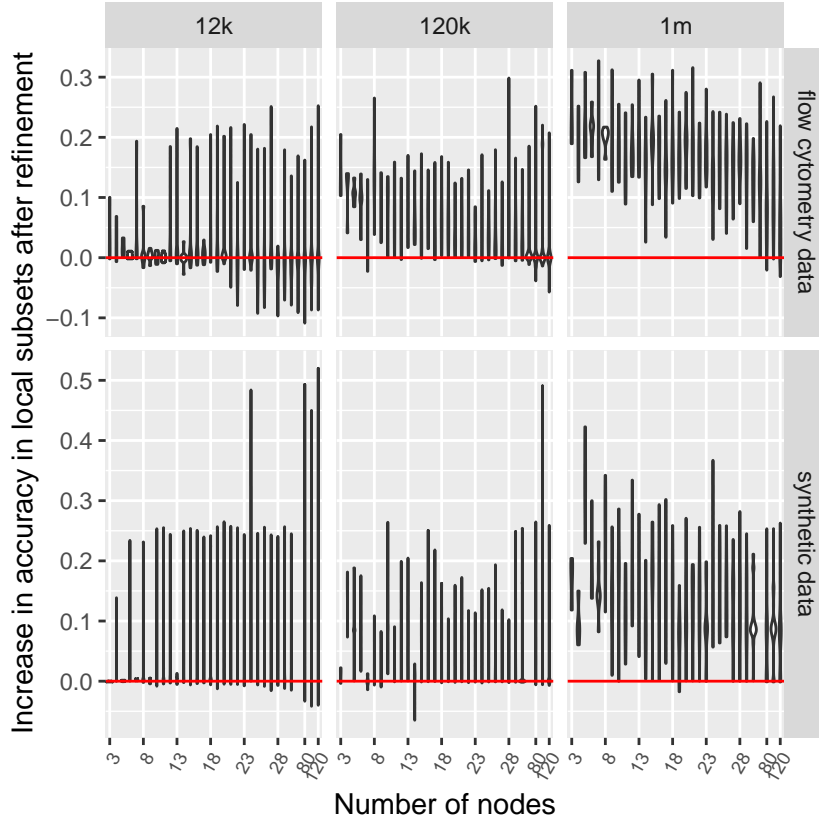


Figure 4: Increase in classification accuracy after refinement in local subsets of the training sets from the flow cytometry (top row) and the synthetic data (bottom row). 12k, 120k and 1m indicate the data size of the training sets. For each data and node setting, we randomly select one of ten replicates and include a violin plot of R statistics, where R is the number of slave nodes (or subsets).

4.2 Results

This section includes experiment results for both the synthetic and flow cytometry data. Reported results include benefits from the local clustering refinement algorithm, classification performance, simulations from the posterior predictive distributions, and computation times.

The classification performance is evaluated for both the training and test sets by three frequently used cluster validation metrics — accuracy, adjusted Rand index (ARI) and F-measure; see Appendix B for definitions. When two partitions agree perfectly, accuracy, ARI and F-measure take value 1; in general, higher values of these statistics represent better clustering performance.

To evaluate the test set performance, we first find an optimal mapping between the labels of the clustering estimates of the training set and the manually-gated labels by minimizing the number of mismatches, so that each label refers to the same cluster in both the training and test set. The extra clusters identified in the estimates are coded as *unknown1*, *unknown2* and so on.

All results, unless explicitly stated, are averaged across 10 replicated experiments.

4.2.1 Benefits from local cluster refinement algorithm

The local cluster refinement algorithm is more than a procedure for cluster label alignment; its general ability to improve the clustering performance for each subset is illustrated by

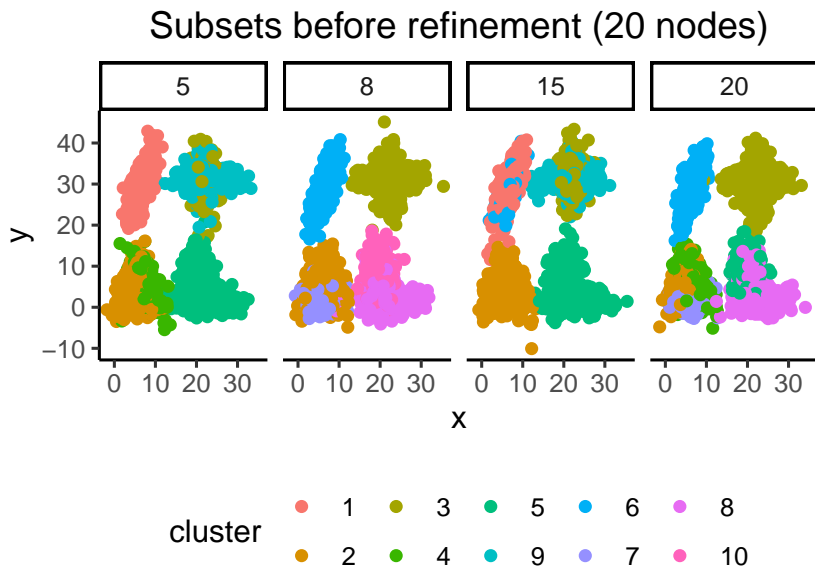
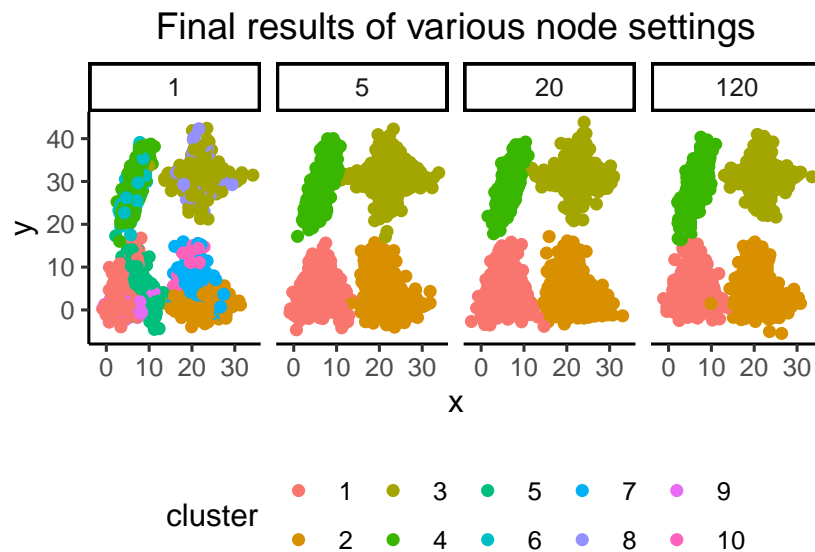


Figure 5: Scatter plots of clustering results associated with the training set of one of the synthetic data sets; the training set contains 1 million observations. The top row represents the final clustering results when the data are randomly distributed to 1, 5, 20 and 120 nodes respectively. The bottom row shows subsets results associated with the 20 nodes in the top row; specifically, it represents clustering results of subset 5, 8, 15 and 20 before local cluster refinement.

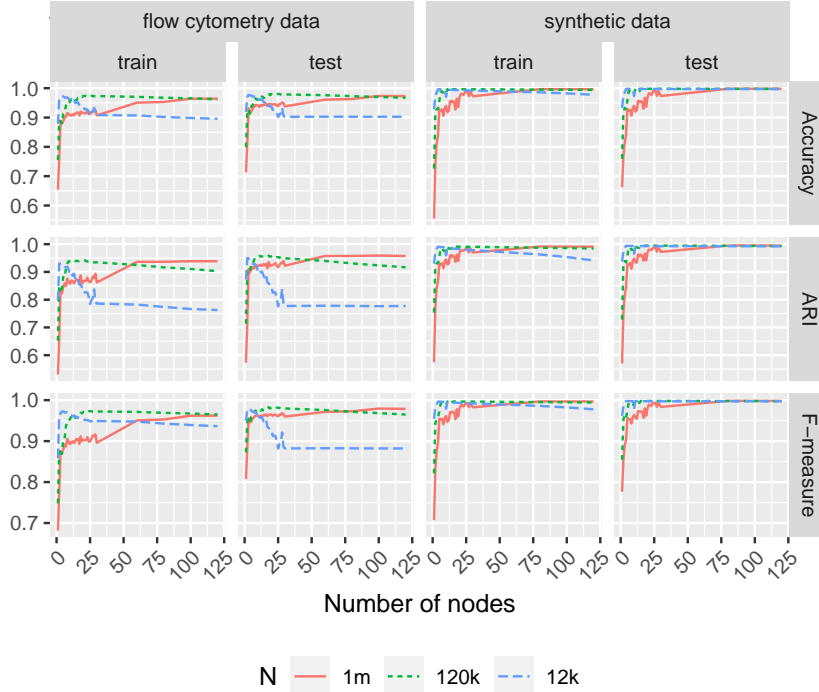


Figure 6: Classification performance of the training and test sets associated with the synthetic (right) and flow cytometry (left) data, as measured by accuracy, ARI, and F-measure.

Figure 4 and 5. Figure 4 illustrates the increase in accuracy associated with the subsets after the local refinement procedure. Specifically, for each node setting, we randomly select a run from the ten replicates and draw a violin plot of the changes in accuracy associated with each subset. The before-refinement accuracy is identified by the optimal iteration that minimizes the expected loss locally, whereas the after-refinement accuracy is identified by the final clustering results mapped to local subsets. We notice a general gain in accuracy, which is especially prominent for the flow cytometry data with $N = 1$ million.

The benefits from local cluster refinement is also corroborated by Figure 5, which shows clustering results of selected subsets before refinement (in the bottom row) and the entire data set after refinement (in the top row) using 20 nodes. The spurious clusters, coming in various shapes and locations, are identified in local subsets but they all vanish in the final cluster estimate.

4.2.2 Classification performance

DIB-C exhibits promising classification performance, as measured by accuracy, ARI and F-measure, for both training and test sets, with results illustrated in Figure 5, 6, 7 and Table 1. Figure 6 shows that these measures are robust to the growing number of nodes for large (i.e. $N = 120k$ and $1m$) data sets; in fact, they increase steadily for the data sets with 1 million observations as the number of nodes increases to 120, likely due to the improved mixing of Markov chain Monte Carlo as the sample sizes per node drop. This may also explain the sharp rises in performance as we increase the number of nodes from one to two. These observations indicate a win-win position: DIB-C is not only scalable, but also robust to the increasing number of nodes. Figure 5 and 7 show the scatter plots of the clustering results associated with a training set of the synthetic data and a test set of the flow cytometry data, respectively, when $N = 1$ million. As evidenced by both figures, the clustering tends to be less noisy and visually more reasonable as the number of nodes increases. In Figure 7, the names of the species overall match their manually-gated labels when the number of nodes is large, with *synecho*, which presents disconnectedness, decomposed into two clusters.

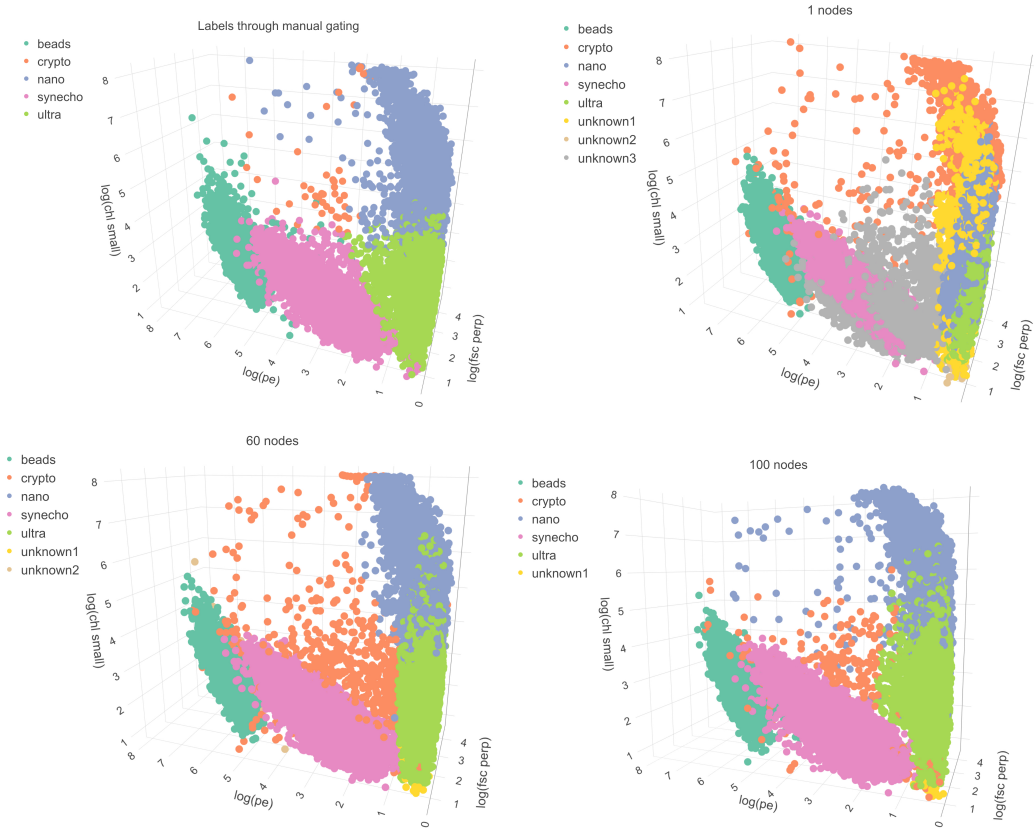


Figure 7: Scatter plots of clustering results of the test set associated with $N = 1$ million data size setting. The top left plot corresponds to the manually-gated labels. The remaining four represent the clustering results from using 1, 60 and 100 nodes respectively. In each scatter plot, only a random subset of the data points are included; and the x , y and z coordinates are $\log(\text{side scatter})$, $\log(\text{orange fluorescence})$ and $\log(\text{red fluorescence})$, respectively. These three explain the most variation in the data among the four variables (according to principle component analysis results).

We have also compared DIB-C with popular distributed clustering algorithms, including DBSCAN (density-based spatial clustering of applications with noise) and K-means. In terms of the tuning parameters, for DBSCAN, we set ϵ based on a widely used k-nearest neighbour distance plot and minPts at the value that maximizes the accuracy, ARI and F-measure for the training set (they all happen to be maximized by the same minPts); for K-means, we set the number of clusters to be 5 (the truth according to the manual gating), 6 and 8 respectively. The distributed version of DBSCAN and K-means are much faster than DIB-C and yield the same clustering performance as their non-distributed counterparts. Yet their performance, as shown in Table 1, is very sensitive to tuning parameters; taking K-means as an example, the slight deviation of K from the truth leads to drastically worse performance. In addition, DIB-C, for which the median performance statistics are reported, consistently outperforms all methods with the exception of K-means when the number of clusters is correctly specified. However, even K-means with the number of clusters correctly specified cannot provide a generative model, based on which we can simulate similar data and perform density estimation and other inference. Our method, however, enjoys such an advantage, as is shown in Section 4.2.3.

We also attempted comparison with Dirichlet-process Gaussian mixtures, another widely used model-based approach for clustering. Since the computation was already extremely slow for $N = 12k$ (taking over 20 hours), we dropped the comparison.

Table 1: The clustering performance of the flow cytometry data across various methods for $N = 12k, 120k$ and $1m$. In particular, the performance of DBSCAN and K-means are invariant to the number of nodes. For DIB-C, the median of each statistic obtained from using varying number of nodes is reported. Yellow and green indicate the best and the second best performance under each scenario respectively.

		train			test		
		Accuracy	ARI	F-measure	Accuracy	ARI	F-measure
12k	DIB-C	0.938	0.849	0.955	0.939	0.860	0.933
	DBSCAN- default	0.719	0.350	0.691	0.716	0.352	0.687
	DBSCAN-optimal (minPts = 40)	0.909	0.803	0.895	0.906	0.790	0.882
	K-means, $K = 5$	0.977	0.945	0.980	0.976	0.941	0.979
	K-means, $K = 6$	0.699	0.593	0.796	0.714	0.603	0.809
	K-means, $K = 8$	0.621	0.537	0.748	0.638	0.547	0.761
120k	DIB-C	0.966	0.938	0.971	0.965	0.952	0.976
	DBSCAN-default	0.904	0.793	0.886	0.903	0.792	0.885
	DBSCAN-optimal (minPts = 5)	0.904	0.793	0.886	0.904	0.792	0.884
	K-means, $K = 5$	0.979	0.950	0.982	0.979	0.950	0.982
	K-means, $K = 6$	0.706	0.706	0.803	0.707	0.707	0.802
	K-means, $K = 8$	0.625	0.543	0.751	0.625	0.546	0.70
1m	DIB-C	0.913	0.868	0.901	0.943	0.924	0.962
	DBSCAN-default	0.718	0.356	0.692	0.718	0.356	0.691
	DBSCAN-optimal (minPts = 12)	0.904	0.791	0.885	0.904	0.791	0.885
	K-means, $K = 5$	0.979	0.949	0.982	0.978	0.948	0.981
	K-means, $K = 6$	0.708	0.599	0.803	0.708	0.599	0.804
	K-means, $K = 8$	0.630	0.544	0.755	0.630	0.544	0.755

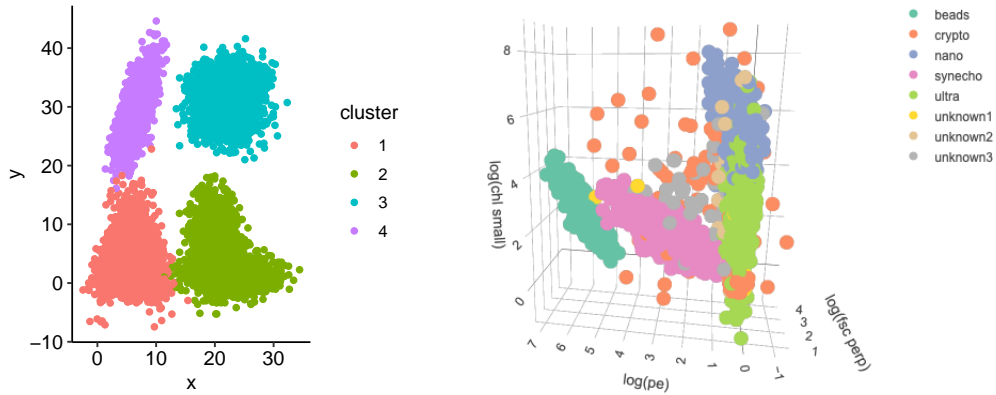


Figure 8: Scatter plots of 10,000 data points simulated from the posterior predictive distributions resulting from an analysis conducted with data distributed across 40 nodes for the synthetic data (left) and the flow cytometry data (right).

4.2.3 Simulation from posterior predictive

Figure 8 shows scatter plots of 10,000 data points simulated from the posterior predictive distributions resulting from analyses in which the synthetic and the flow cytometry data are randomly distributed across 40 nodes. The posterior predictive distributions show striking resemblance to the true data; the cluster labels, mapped to the true labels by minimizing number of mismatches during the training phase, also largely match those in the original data set.

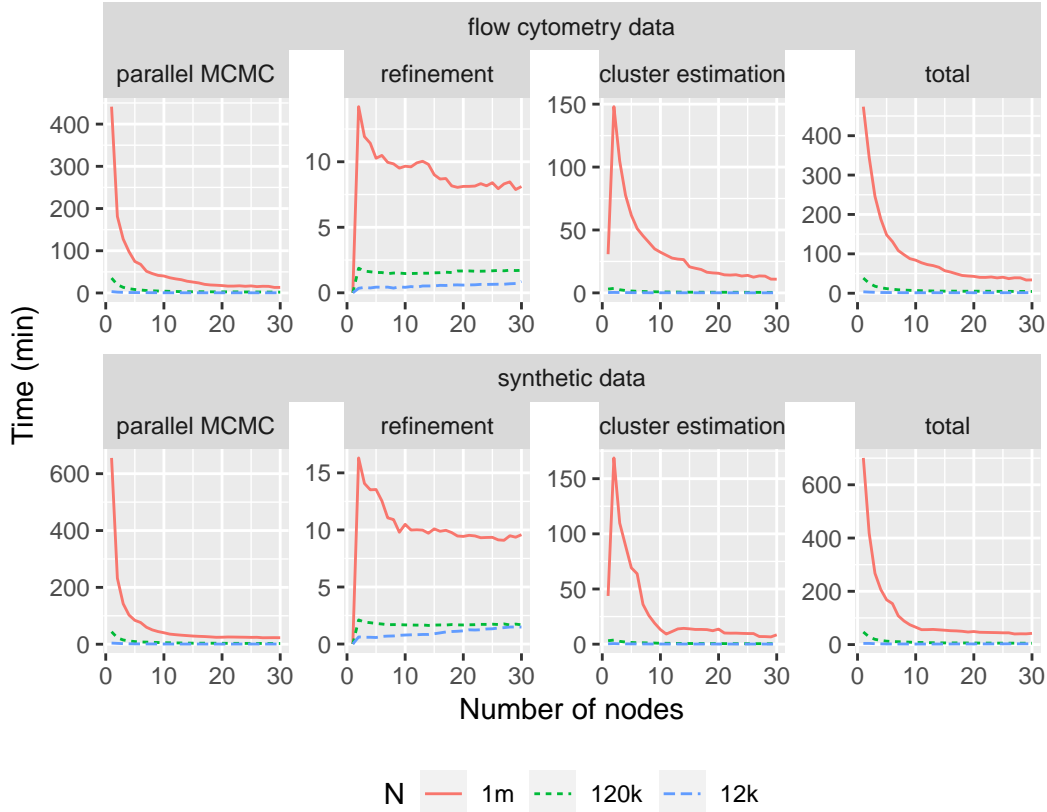


Figure 9: The computation time of the synthetic data (bottom) and flow cytometry data (top) of the training sets. For each data setting, we include total computation (the fourth col.), parallel MCMC for local clustering (the first col.), local cluster refinement (the second col.) and global cluster estimation time (the third col.)

4.2.4 Computation time

Figure 9 displays the computation time for parallel MCMC, local cluster refinement, global cluster estimation and the total run time, respectively. We notice similar trends in both data settings, most notably the drastic decrease in the total computation time of the data sets with one million observations; the dive, quickly plateauing at around 15 nodes, is mostly attributable to a significant speedup, dropping from around 8.5 hours to 15 minutes, from parallel MCMC. No refinement or global cluster estimation is necessary in a conventional single machine scenario, which explains the jump in the associated time when switching to two nodes.

5 Conclusion

In this paper, we have proposed a nearly embarrassingly parallel framework named DIB-C for distributed Bayesian clustering. DIB-C accommodates any loss function on the space of partitions for cluster estimation, quickly classifies future subjects, and allows density estimation and other posterior inference. Our extensive experiments also demonstrate that DIB-C is not only scalable, but also robust to the increasing number of nodes for large data sets.

Acknowledgement

The authors acknowledge support from SAS Institute Inc., United States National Science Foundation grant 1546130 and National Institute of Environmental Health Sciences of the National Institutes of Health grant R01ES027498.

References

- Armbrust Lab. IAAI SeaFlow Challenge Data Sets. Available from <https://github.com/jhyrkas/iaai-challenge-data>.
- Jean-Patrick Baudry, Adrian E Raftery, Gilles Celeux, Kenneth Lo, and Raphaël Gottardo. Combining mixture components for clustering. *J Comput Graph Stat.*, 9(2):332–353, 2010. URL [doi:10.1198/jcgs.2010.08111](https://doi.org/10.1198/jcgs.2010.08111).
- D. A. Binder. Bayesian cluster analysis. *Biometrika*, 65(1):31–38, 1978. doi: 10.1093/biomet/65.1.31. URL <http://dx.doi.org/10.1093/biomet/65.1.31>.
- L. Hubert and P. Arabie. Comparing partitions. *Journal of classification*, 2(1):193–218, 1985. URL <http://scholar.google.de/scholar.bib?q=info:IkrWWF2JxwoJ:scholar.google.com/&output=citation&hl=de&ct=citation&cd=0>.
- Jeremy Hyrkas, Sophie Clayton, Francois Ribalet, Daniel Halperin, E. Virginia Armbrust, and Bill Howe. Scalable clustering algorithms for continuous environmental flow cytometry. *Bioinformatics*, 32(3):417–423, 10 2015. ISSN 1367-4803. doi: 10.1093/bioinformatics/btv594. URL <https://doi.org/10.1093/bioinformatics/btv594>.
- Jeremy Hyrkas, Sophie Clayton, Francois Ribalet, Daniel Halperin, E. Virginia Armbrust, and Bill Howe. Scalable clustering algorithms for continuous environmental flow cytometry. *Bioinformatics*, 32(3):417–423, 2016. doi: 10.1093/bioinformatics/btv594. URL <http://dx.doi.org/10.1093/bioinformatics/btv594>.
- Eshref Januzaj, Hans-Peter Kriegel, and Martin Pfeifle. Scalable density-based distributed clustering. In *Proceedings of the 8th European Conference on Principles and Practice of Knowledge Discovery in Databases*, PKDD '04, pages 231–244, New York, NY, USA, 2004. Springer-Verlag New York, Inc. ISBN 3-540-23108-0. URL <http://dl.acm.org/citation.cfm?id=1053072.1053095>.
- Ramesh M. Korwar and Myles Hollander. Contributions to the theory of dirichlet processes. *Ann. Probab.*, 1(4):705–711, 08 1973. doi: 10.1214/aop/1176996898. URL <https://doi.org/10.1214/aop/1176996898>.
- Cheng Li, Sanvesh Srivastava, and David B. Dunson. Simple, scalable and accurate posterior interval estimation. *Biometrika*, 104(3):665–680, 2017. doi: 10.1093/biomet/asx033. URL <http://dx.doi.org/10.1093/biomet/asx033>.
- Gertraud Malsiner-Walli, Sylvia Frühwirth-Schnatter, and Bettina Grün. Identifying mixtures of mixtures using Bayesian estimation. *Journal of Computational and Graphical Statistics*, 26(2):285–295, 2017. doi: 10.1080/10618600.2016.1200472. URL <https://doi.org/10.1080/10618600.2016.1200472>.
- Marina Meilă. Comparing clusterings—an information based distance. *Journal of Multivariate Analysis*, 98(5):873 – 895, 2007. ISSN 0047-259X. doi: <https://doi.org/10.1016/j.jmva.2006.11.013>. URL <http://www.sciencedirect.com/science/article/pii/S0047259X06002016>.
- Jeffrey W. Miller and Matthew T. Harrison. Inconsistency of Pitman-Yor process mixtures for the number of components. *Journal of Machine Learning Research*, 15:3333 – 3370, 2014.
- Stanislav Minsker, Sanvesh Srivastava, Lizhen Lin, and David Dunson. Scalable and robust Bayesian inference via the median posterior. In Eric P. Xing and Tony Jebara, editors, *Proceedings of the 31st International Conference on Machine Learning*, volume 32 of *Proceedings of Machine Learning Research*, pages 1656–1664, Beijing, China, 22–24 Jun 2014. PMLR. URL <http://proceedings.mlr.press/v32/minsker14.html>.
- Willie Neiswanger, Chong Wang, and Eric P. Xing. Asymptotically exact, embarrassingly parallel mcmc. In *Proceedings of the Thirtieth Conference on Uncertainty in Artificial Intelligence*, UAI'14, pages 623–632, Arlington, Virginia, United States, 2014. AUAI Press. ISBN 978-0-9749039-1-0. URL <http://dl.acm.org/citation.cfm?id=3020751.3020816>.

- Yang Ni, Peter Müller, Maurice Diesendruck, Sinead Williamson, Yitan Zhu, and Yuan Ji. Scalable Bayesian nonparametric clustering and classification. *arXiv preprint: 1806.02670v1*, 2018.
- Peter Orbanz. Lecture notes on Bayesian nonparametrics, May 2014. URL http://stat.columbia.edu/~porbanz/papers/porbanz_BNP_draft.pdf.
- S. Papadimitriou and J. Sun. Disco: Distributed co-clustering with map-reduce: A case study towards petabyte-scale end-to-end mining. In *2008 Eighth IEEE International Conference on Data Mining*, pages 512–521, Dec 2008. doi: 10.1109/ICDM.2008.142.
- Panagiotis Papastamoulis. Handling the label switching problem in latent class models via the ecr algorithm. *Communications in Statistics - Simulation and Computation*, 43(4): 913–927, 2014. doi: 10.1080/03610918.2012.718840. URL <https://doi.org/10.1080/03610918.2012.718840>.
- Panagiotis Papastamoulis and George Iliopoulos. An artificial allocations based solution to the label switching problem in bayesian analysis of mixtures of distributions. *Journal of Computational and Graphical Statistics*, 19(2):313–331, 2010. doi: 10.1198/jcgs.2010.09008. URL <https://doi.org/10.1198/jcgs.2010.09008>.
- Carlos E. Rodríguez and Stephen G. Walker. Label switching in bayesian mixture models: Deterministic relabeling strategies. *Journal of Computational and Graphical Statistics*, 23(1):25–45, 2014. doi: 10.1080/10618600.2012.735624. URL <https://doi.org/10.1080/10618600.2012.735624>.
- Judith Rousseau and Kerrie Mengersen. Asymptotic behaviour of the posterior distribution in overfitted mixture models. *Journal of the Royal Statistical Society: Series B (Statistical Methodology)*, 73(5):689–710, 2011.
- Steven L. Scott, Alexander W. Blocker, Fernando V. Bonassi, Hugh A. Chipman, Edward I. George, and Robert McCulloch. Bayes and big data: The consensus monte carlo algorithm. *International Journal of Management Science and Engineering Management*, 11(2):78–88, 2016. ISSN 1750-9653. doi: 10.1080/17509653.2016.1142191.
- Heidi M. Sosik, Robert J. Olson, and E. Virginia Armbrust. *Flow Cytometry in Phytoplankton Research*, pages 171–185. Springer Netherlands, Dordrecht, 2010. ISBN 978-90-481-9268-7. doi: 10.1007/978-90-481-9268-7_8. URL https://doi.org/10.1007/978-90-481-9268-7_8.
- M. Sperrin, T. Jaki, and E. Wit. Probabilistic relabelling strategies for the label switching problem in bayesian mixture models. *Statistics and Computing*, 20(3):357–366, Jul 2010. ISSN 1573-1375. doi: 10.1007/s11222-009-9129-8. URL <https://doi.org/10.1007/s11222-009-9129-8>.
- Sanvesh Srivastava, Volkan Cevher, Quoc Dinh, and David Dunson. WASP: Scalable Bayes via barycenters of subset posteriors. In Guy Lebanon and S. V. N. Vishwanathan, editors, *Proceedings of the Eighteenth International Conference on Artificial Intelligence and Statistics*, volume 38 of *Proceedings of Machine Learning Research*, pages 912–920, San Diego, California, USA, 09–12 May 2015. PMLR. URL <http://proceedings.mlr.press/v38/srivastava15.html>.
- Matthew Stephens. Dealing with label switching in mixture models. *Journal of the Royal Statistical Society. Series B (Statistical Methodology)*, 62(4):795–809, 2000. ISSN 13697412, 14679868. URL <http://www.jstor.org/stable/2680622>.
- Sara Wade and Zoubin Ghahramani. Bayesian cluster analysis: Point estimation and credible balls. *Bayesian Analysis*, 2017.
- Xiangyu Wang, Fangjian Guo, Katherine A Heller, and David B Dunson. Parallelizing MCMC with random partition trees. In C. Cortes, N. D. Lawrence, D. D. Lee, M. Sugiyama, and R. Garnett, editors, *Advances in Neural Information Processing Systems 28*, pages 451–459. Curran Associates, Inc., 2015. URL <http://papers.nips.cc/paper/5986-parallelizing-mcmc-with-random-partition-trees.pdf>.

Weizhong Zhao, Huifang Ma, and Qing He. Parallel K-means clustering based on MapReduce. In Martin Gilje Jaatun, Gansen Zhao, and Chunming Rong, editors, *Cloud Computing*, pages 674–679, Berlin, Heidelberg, 2009. Springer Berlin Heidelberg. ISBN 978-3-642-10665-1.

A MCMC sampling scheme

We adapt Wade and Ghahramani [2017]’s MCMC sampling scheme for finite mixture of mixtures for the embarrassingly parallel MCMC framework of PIE. Assume \mathcal{Y} can be partitioned into R non-overlapping subsets, with subset r , denoted by \mathcal{Y}_r , residing on worker node r ($r = 1, \dots, R$). For each subset, estimation of a sparse hierarchical mixture of mixtures model is performed through MCMC sampling based on data augmentation and Gibbs sampling.

Without loss of generality, we introduce the Gibbs sampling steps based on subset posterior r , in which subset likelihood is raised to the power of $a := N/N_r \approx R$ to ensure that the variance of each subset posterior is roughly on the same scale as that of the overall posterior. Let $\mathbf{c}_r = (c_1, \dots, c_{N_r})$ be the latent cluster allocation variable, which take values in $\{1, \dots, K\}^{N_r}$, indicating the cluster to which each observation belongs such that

$$p(y_i|\theta_1, \dots, \theta_K, c_i = k) = p_k(y_i|\theta_k), \quad \text{and} \quad P\{c_i = k|\eta\} = \eta_k.$$

Additionally, we introduce latent allocation variables $\mathbf{s}_r = (s_1, \dots, s_{N_r})$, which take values in $\{1, \dots, L\}^{N_r}$, to indicate the subcomponent to which an observation within a cluster is assigned such that

$$p_k(y_i|\theta_k, c_i = k, s_i = l) = f_N(y_i|\mu_{kl}, \Sigma_{kl}), \quad \text{and} \quad Pr\{s_i = l|c_i = k, w_k\} = \omega_{kl}.$$

Based on the priors specified before, with fixed hyperparameters (e_0, d_0, c_0) , the latent $(\mathbf{c}_r, \mathbf{s}_r)$ and parameters $(\eta, \omega_k, \mu_{kl}, \Sigma_{kl}, C_{0k}, b_{0k}, \lambda_{kj})$, $k = 1, \dots, K$, $l = 1, \dots, L$, $j = 1, \dots, d$, are sampled from the *subset posterior* using the following Gibbs sampling scheme. The sampler alternates between updating cluster weights η , imputing latent cluster allocation \mathbf{c}_r , and updating cluster-specific parameters, which constitutes sampling for subcomponents within each cluster.

1. Sampling steps on the level of the cluster distribution:

- (a) Parameter simulation step conditional on the classification \mathbf{c}_r . Sample $\eta|\mathbf{c}_r$ from $\text{Dir}(e_1, \dots, e_K)$, $e_k = e_0 + an_k$, $k = 1, \dots, K$, where $n_k = \#\{i : c_i = k\}$ is the number of observations allocated to cluster k .
- (b) Classification step for each observation y_i conditional on cluster-specific parameters. For each $i = 1, \dots, N_r$ sample the cluster assignment c_i from

$$P\{c_i = k|y_i, \theta, \eta\} \propto \eta_k p_k(y_i|\theta_k), k = 1, \dots, K,$$

where $p_k(y_i|\theta_k)$ is the semi-parametric mixture approximation of the cluster density:

$$p_k(y_i|\theta_k) = \sum_{l=1}^L w_{kl} f_N(y_i|\mu_{kl}, \Sigma_{kl}).$$

2. Within each cluster k , $k = 1, \dots, K$:

- (a) Classification step for all observations y_i , assigned to cluster k (i.e. $c_i = k$), conditional on the subcomponent weights and the subcomponent-specific parameters. For each $i \in \{i = 1, \dots, N_r : c_i = k\}$ sample s_i from

$$Pr\{s_i = l|y_i, \theta_k, c_i = k\} \propto w_{kl} f_N(y_i|\mu_{kl}, \Sigma_{kl}), l = 1, \dots, L$$

- (b) Parameter simulation step conditional on the classifications \mathbf{s}_r and \mathbf{c}_r :
 - i. Sample $w_k|\mathbf{c}_r, \mathbf{s}_r$ from $\text{Dir}(d_{k1}, \dots, d_{kL})$, $d_{kl} = d_0 + a \times n_{kl}$, $l = 1, \dots, L$, where $n_{kl} = \#\{i : s_i = l, c_i = k\}$ is the number of observations allocated to subcomponent l in cluster k .
 - ii. For $l = 1, \dots, L$: Sample $\Sigma_{kl}^{-1}|\mathbf{c}_r, \mathbf{s}_r, \mu_{kl}, C_{0k}, y \sim W_d(c_{kl}, C_{kl})$, where

$$c_{kl} = c_0 + a \times n_{kl},$$

$$C_{kl} = C_{0k} + a \sum_{i:s_i=l, c_i=k} (y_i - \mu_{kl})(y_i - \mu_{kl})^T$$

iii. For $l = 1, \dots, L$: Sample $\mu_{kl} | \mathbf{c}_r, \mathbf{s}_r, b_{0k}, \Sigma_{kl}, \Lambda_k, y \sim N_d(b_{kl}, B_{kl})$, where

$$B_{kl} = (\tilde{B}_{0k}^{-1} + an_{kl}\Sigma_{kl}^{-1})^{-1},$$

$$b_{kl} = B_{kl}(\tilde{B}_{0k}^{-1}b_{0k} + \Sigma_{kl}^{-1}n_{kl}\bar{y}_{kl}),$$

with $\tilde{B}_{0k} = \sqrt{\Lambda_k}B_0\sqrt{\Lambda_k}$, $\Lambda_k = \text{diag}(\lambda_{k1}, \dots, \lambda_{kd})$, and $\bar{y}_{kl} = 1/n_{kl} \sum_{i, s_i=l, c_i=k} y_i$ being equal to the subcomponent mean for $n_{kl} > 0$ and $n_{kl}\bar{y}_{kl} = 0$, otherwise.

3. **For each cluster $k, k = 1, \dots, K$: Sample the random hyperparameters $\lambda_{kj}, C_{0k}, b_{0k}$ from their full conditionals:**

(a) For $j = 1, \dots, d$: Sample $\lambda_{kj} | b_{0k}, \mu_{k1}, \dots, \mu_{kL} \sim \text{GIG}(p_{kL}, a_{kj}, b_{kj})$, where GIG is the generalized inverse Gaussian distribution and

$$p_{kL} = -L/2 + \nu,$$

$$a_{kj} = 2\nu,$$

$$b_{kj} = \sum_{l=1}^L (\mu_{kl,j} - b_{0k,j})^2 / B_{0,jj}.$$

(b) Sample $C_{0k} | \Sigma_{k1}, \dots, \Sigma_{kL} \sim W_d(g_0 + Lc_0, G_0 + \sum_{l=1}^L \Sigma_{kl}^{-1})$.

(c) Sample $b_{0k} | \tilde{B}_{0k}, \mu_{k1}, \dots, \mu_{kL} \sim N_d(\tilde{m}_k, \tilde{M}_k)$, where

$$\tilde{M}_k = (M_0^{-1} + L\tilde{B}_{0k}^{-1})^{-1},$$

$$\tilde{m}_k = \tilde{M}_k \left(M_0^{-1}m_0 + \tilde{B}_{0k}^{-1} \sum_{l=1}^L \mu_{kl} \right).$$

B Definition of clustering validation metrics

Write true positive, true negative, false positive and false negative as TP, TN, FP and FN respectively.

The definition of accuracy, F-measure and adjusted rand index is given as follows:

1. Accuracy

$$\text{Accuracy} = \frac{\#\text{TP} + \#\text{TN}}{\#\text{observations}}$$

2. F-measure

Precision and Recall are defined as follows:

$$\text{Precision} = \frac{\#\text{TP}}{\#\text{TP} + \#\text{FP}}, \quad \text{and} \quad \text{Recall} = \frac{\#\text{TP}}{\#\text{TP} + \#\text{FN}}$$

F-measure is the harmonic mean of precision of recall:

$$\text{F-measure} = 2 \cdot \frac{\text{precision} \cdot \text{recall}}{\text{precision} + \text{recall}}$$

3. Adjusted rand index (ARI)

Adjusted rand index is a corrected-for-chance version of Rand index, the definition of which is similar to accuracy. See Hubert and Arabie [1985] for a formal definition of adjusted rand index.